

13  
**Structural and field emission properties of effective nanocomposite cathodes CNT@TiO<sub>2</sub>**

© M.A. Chumak,<sup>1</sup> E.O. Popov,<sup>1</sup> S.V. Filippov,<sup>1</sup> A.G. Kolosko,<sup>1</sup> E.V. Zhizhnik,<sup>2</sup> A.V. Koroleva,<sup>2</sup> L.A. Filatov,<sup>3</sup> I.S. Ezhov,<sup>3</sup> M.Yu. Maximov<sup>3</sup>

<sup>1</sup> Ioffe Institute, St. Petersburg, Russia

<sup>2</sup> St. Petersburg State University, St. Petersburg, Russia

<sup>3</sup> Peter the Great Saint-Petersburg Polytechnic University, St. Petersburg, Russia

e-mail: equilibrium2027@yandex.ru.

Received March 14, 2024

Revised April 24, 2024

Accepted April 25, 2024

A comprehensive study of the composition and field emission properties of field emission cathodes based on CNT@TiO<sub>2</sub> core-shell nanocomposites is presented. Coatings with arrays of vertical carbon nanotubes (CNTs) were produced by the plasma-chemical method on silicon substrates with a Ni catalyst, and thin layers of TiO<sub>2</sub> were produced by subsequent atomic layer deposition. It was found that the work function of the coating material with the initial CNT array was 4.98 eV; for the case of CNT@TiO<sub>2</sub>, it took values of 4.29 and 3.82 eV for oxide thicknesses of 3 and 6 nm, respectively. The developed technique for comparing emission characteristics showed that a decrease in the work function of structures with CNT@TiO<sub>2</sub> was accompanied by a decrease in local electric fields at the tips. A cathode with CNT@TiO<sub>2</sub> arrays (6 nm) required the lowest electric field in the group of samples to ensure an emission current density of 1 mA/cm<sup>2</sup> about 5 · 10<sup>9</sup> V/m. This is 1.6 times less than for a similar sample with an array of „pure“ CNTs. The average values of the effective field enhancement coefficient tended to decrease when going from CNTs to CNTs@TiO<sub>2</sub>, probably due to an increase in the radius of curvature of tubular nanoparticles upon deposition of an additional layer. Modification with an oxide coating led to an increase in the effective emission area of the cathode.

**Keywords:** field emission, nanocomposite, carbon nanotube array, TiO<sub>2</sub> thin films, X-ray photoelectron spectroscopy, atomic layer deposition, plasma chemical deposition, work function.

DOI: 10.61011/TP.2024.06.58831.85-24

## Introduction

Owing to a unique complex of their physical and electrophysical properties, carbon nanotubes (CNTs) are a promising material for design of various devices operated on a field emission effect. Prototypes of a vacuum switch [1], a discharge arrester [2], X-ray emitters [3–6], a full-color display [7,8], lighting systems [9,10], a disinfectant ultraviolet lamp [11], touch and pressure sensors [12,13] etc. on their basis were considered. But there are restrictions preventing wide use of field cathodes based on CNT. Besides, they often mention a relatively high threshold field, moderate parameters of emission homogeneity in the cathode surface area, stability of its emission and long-term strength of its operation. According to data from a series of specialized papers, improvement of the noted CNT parameters may be achieved by different methods for surface processing, for example, plasma, laser and ionic exposure [14–18]. Besides, ample opportunities are provided by application of additional coatings, first of all from metal oxides.

Usually coatings are used from materials with low work function. However, analysis of thin coatings based on wide-band materials is of interest as well without any doubt. Cathodes from CNT with thin layers of oxides show

reduction in the value of emission threshold field, increased homogeneity of emission and operation stability. This was observed on the examples of ZnO [19,20], MgO [21], FeOx [22], RuO<sub>2</sub> [23,24], CuO [25], NiO [26], IrO<sub>2</sub> [27,28], HfO<sub>2</sub> [29]. In particular, autoemission properties are improved significantly after application of a coating from TiO<sub>2</sub> by sol-gel method [30]. CNT-based layers had threshold field of  $E_{th}$  1.257 V/μm, and with CNT/TiO<sub>2</sub> structures it decreased down to 0.657 V/μm. Morphology variation analysis made it possible to conclude on the reduction of mutual screening from points of a nanocomposite CNT/TiO<sub>2</sub> cathode. Besides, the outer layer of TiO<sub>2</sub> demonstrated resistance to oxygen ions produced in the measurement chamber due to residual atmosphere. The found high stability of the sample electronic emission is also related to this fact. Increased stability for CNT/TiO<sub>2</sub> structures is also shown in [31], where the compound was deposited otherwise — by chemical gas phase method. A smaller switching field was required for them as well. Increased electron emission correlated with increased field gain factor, which the authors related to the special structure of TiO<sub>2</sub> nanoparticles on the CNT surface. Research results [32] demonstrated that a CNT/TiO<sub>2</sub>:N composite may be a more promising candidate for field emission devices. Combined geometric structure and effects of low affinity to TiO<sub>2</sub>

electron alloyed with nitrogen in the TiO<sub>2</sub>/CNT composite resulted in a low electric field 1.0 V/μm at emission current density 10 μA/cm<sup>2</sup>, high gain factor of the field 3.0 · 10<sup>3</sup> and field emission stability.

Great importance is attached to the field radiating cathode material work function as a key factor influencing the field emission efficiency. The lower the work function, the lower the potential barrier at the boundary between the material and vacuum, the smaller electric field is necessary to tunnel the electrons into vacuum. The wide spread of work function values observed in practice for each specific material is caused by the fact that the parameter is very sensitive to some factors inherent in real systems. Such factors as surface roughness [33,34], open crystal face [35], and coating with adsorbates [36] impact the dipole component of the surface, while the chemical potential of electrons is affected by the chemical identity of the material, availability of admixtures and stoichiometry of the material [37]. Metal oxides demonstrate alloying asymmetry [38]. It means that some oxides tend to form one type of defects vs the other one. Due to their own defects many oxides may have a nature of either *n*-, or *p*-type. Impact of vacancies at an electron structure MoO<sub>3</sub> was visually demonstrated by the authors of paper [37], which tracked impact of oxygen deficit in the structure of film MoO<sub>3-x</sub> at its work function and composition of the valence band. Reduction of work function was shown as the vacancies increased in the film structure. In [39] it was also demonstrated that due to availability of many defects in the form of oxygen vacancies in a NiO structure, the work function may reduce down to 4.26 eV. Therefore, to study the laws of field emission in nanocomposite cathodes being CNTs coated with nanometer films of metal oxides, it is relevant to control chemical and electron structure, in particular work function, cathode structures.

Thus, multiple papers noted positive effect of metal oxide coatings, in particular, TiO<sub>2</sub>, on field emission of CNTs causing reduction of the emission threshold field and emission current stabilization. Most data available in the literature on this type of nanocomposites is concentrated on searching for a new oxide coating to combine with a CNT or to expand of already known structures into more complicated systems. However, detailed research of structural and electronic features of metal oxides, as well as identification of the nature of their correlation with the improved field emission characteristics of CNT/metal oxide nanocomposites are yet underrepresented.

This paper shows a complex research of structural and emission characteristics of nanocomposite field radiating cathodes based on the structures ordered in a vertical array of „core–shell“ type — CNT@TiO<sub>2</sub>. For their development, a combination of methods to make a composite is suggested, which has not been considered previously for this application: atomic layer deposition (ALD) of catalyst (NiO) for CNT growth, catalytic plasmachemical deposition of arrays of vertical CNTs and subsequent ALD of ultrathin layers of TiO<sub>2</sub>.

## 1. Materials and methods

### 1.1. Manufacturing of structures of CNT/TiO<sub>2</sub> nanocomposite cathodes

Samples of Si/CNT@TiO<sub>2</sub> nanocomposite cathodes were made by serial formation of a catalyst layer from nickel, its growth using CNT arrays and their subsequent decoration with a layer of TiO<sub>2</sub>. To manufacture cathode structures, silicon substrates KDB-10 (100) were used. A nickel catalyst was made via application of a solid thin layer of NiO by ALD method, its chemical and thermal processing to recover nickel and form an island metal film.

#### 1.1.1. Application of NiO

ALD was carried out on „Picosun R-150“ unit (Finland) in a system of reagents bis(cyclopentadienyl)nickel (II)–ozone. Nitrogen (of high purity grade) was used as a carrier gas and a blowdown gas. One cycle of the process may be presented as: supply NiCp<sub>2</sub>/blowdown/supply O<sub>3</sub>/blowdown with duration of stages 1.0/10.0/6.0/10.0 s. Deposition temperature was maintained at the level of 250°C, NiCp<sub>2</sub> sublimation temperature — at 110°C. As it was shown before [40], the thickness of the produced film of catalyst NiO, required for intensive CNT growth, is in the range from 3.5 to 3.9 nm. This paper selected the NiO thickness of 3.8 nm.

#### 1.1.2. Recovery of Ni from NiO

Directly prior to CNT deposition in a reactor for their synthesis the NiO coating was exposed to thermal treatment in atmosphere on the basis of ammonia at subsequent heating to temperature of 680°C and soaking for 5 min. This caused formation of a layer of individual nanoparticles of metal nickel. The recovery atmosphere was created in a working mix of NH<sub>3</sub> (10 ml/min.) and Ar (50 ml/min.) at total pressure of 300 Pa by catalytic decomposition of ammonia on the surface of the nickel oxide layer and recovered nickel.

#### 1.1.3. Growth of CNT arrays

Immediately after the procedure of Ni recovery the nanotubes were deposited. CNT arrays were grown with the help of plasmachemical deposition from a gas phase using a DC discharge. Substrates were placed on a heated cathode made of graphite, the anode was a disc of stainless steel. Both electrodes had ø 45 mm, a gap between them was 40 mm. Deposition lasted for 4 min, the substrate temperature was 680°C, the total pressure of the working medium was 300 Pa. The atmosphere was created from ammonia (135 ml/min) and acetylene (55 ml/min). The discharge is characterized by current 5 mA and voltage 480 V. Additional details of the CNT synthesis method may be found in [40,41].

### 1.1.4. Application of TiO<sub>2</sub> coating on CNT

Thin layers of TiO<sub>2</sub> were grown on substrates with CNT on the already specified ALD unit in a system of reagents of titanium tetroisopropylate (TIPT) — water. One cycle may be presented as: supply of TIPT/blowdown/supply of H<sub>2</sub>O/blowdown, with stage duration of 4/16/1/12 s. Deposition temperature was maintained at the level of 250°C, first reagent evaporation temperature — at 100°C, second one — at 25°C. The formal growth per cycle was around 0.4 Å. To study the effect of TiO<sub>2</sub> on the field emission efficiency, samples were created with CNT arrays without an oxide coating (B1) and with different thickness of TiO<sub>2</sub> (B2 and B3), which formed CNT@TiO<sub>2</sub>. The number of ALD cycles for application of TiO<sub>2</sub> onto CNT was 93 and 186 for B2 samples (thickness of the created oxide is around 3 nm) and B3 (thickness of around 6 nm) accordingly.

## 1.2. Investigation techniques

To analyze the results of CNT array growth, scanning electron microscopy (SEM) was used, a microscope „SUPRA 55VP“ („Carl Zeiss“, Germany). Thin analysis of morphology of individual array elements was conducted with the help of transmission electron microscopy (TEM), microscope „CarlZeissAuriga“ („Carl Zeiss“, Germany). X-ray photoelectron spectroscopy (XPS) was used to study the chemical composition and chemical state of the surface elements in CNT/TiO<sub>2</sub> nanocomposites. A photoelectron spectrometer „Thermo Fisher Scientific Escalab 250Xi“ („Waltham“, Massachusetts, USA) was used, equipped with a source of monochromatic emission AlK<sub>α</sub> (photon energy of 1486.6 eV). The spectrometer was calibrated along the line Au4f<sub>7/2</sub> (binding energy 84.0 eV). To neutralize the sample charge in all dimensions, a combined ion-electron system of charge compensation was used. In this paper the spectra were recorded in the mode of continuous transmittance energy at 50 eV with spot size of 650 μm. Panoramic spectra were recorded with a pitch of 0.50 eV at number of passages equal to 5. High resolution spectra for lines C1s, O1s, Ni2p, Ti2p were recorded with pitch of 0.10 eV at number of passages equal to 25. Studies were conducted at room temperature in ultrahigh vacuum (pressure of not more than 10<sup>-10</sup> mbar). They were calibrated by position of C1s = 284.7 eV. To process spectra, CASAXPS software was used. XPS was also used to measure spectra of valence band and work function of the CNT@TiO<sub>2</sub> nanocomposite surface by cut-off of secondary electrons [42]. Spectra were recorded in the mode of constant transmittance energy at 10 eV, with spot size 650 μm, with pitch 0.10 eV.

For autoemission tests, samples of structures were prepared with surface areas close to 1 cm<sup>2</sup>. The studied nanocomposite cathodes were placed into a vacuum chamber of a specialized unit to measure CVC with a diode system of electrodes. Vacuum of not worse than 5 · 10<sup>-7</sup> Torr was used. Field emission CVC measurements were carried out with an AC source at frequency of

50 Hz, with electrode-to-electrode gap of 370 μm. Detailed description of the unit and measurement method is provided in paper [43].

## 2. Results and discussions

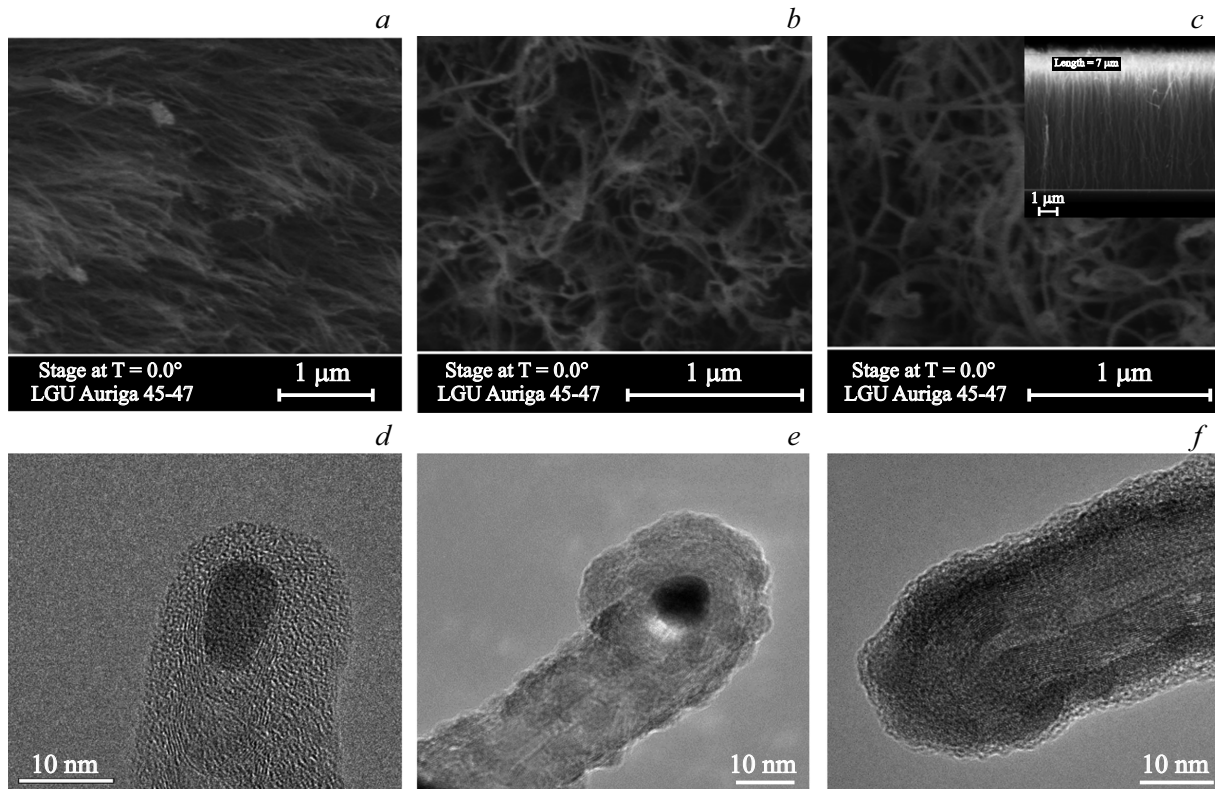
### 2.1. Characterization of CNT/TiO<sub>2</sub> nanocomposite structures

Fig. 1, *a–c* shows SEM images of the surface of three prepared samples, where in general similar morphology is observed for the layer surface from thread-like particles. Control of samples along the cross section demonstrated availability of the array of vertical CNTs with length of around 7 μm (insert in Fig. 1, *c*).

Nanotubes demonstrate loss of preferential orientation only at the very tops. Ultrathin layer of TiO<sub>2</sub> did not impact the nature of thread-like structure arrays based on SEM images. Use of high resolution TEM makes it possible to assess the difference of structures at a thin level. The example of a separate thread-like object of sample B1 (Fig. 1, *d*) shows a nanotube from carbon with a part of catalyst on the top. The average diameter of CNT in the array was 15 nm, the average number of walls from graphene layers was around 20. The tubes of samples B2 and B3 on the surface show an additional layer (Fig. 1, *e, f*). Thinner film of TiO<sub>2</sub> in sample B2 in Fig. 1, *e* has a clearly granular morphology and average thickness of around 3 nm. As the number of ALD cycles increases, a homogeneous coating has already been formed, which you can see in sample B3 with layer thickness of around 6 nm (Fig. 1, *f*).

To study the composition of CNT@TiO<sub>2</sub> nanocomposites, studies of the chemical composition by XPS method were conducted. Spectra of Fig. 2 demonstrate the presence of C, O, Ni and traces of N in all samples. Nickel was used as a catalyst of CNT growth. It is encapsulated as nanoparticles in nanotubes (Fig. 1, *d, e*), and is also distributed on the boundary of the silicon plate (its part that was not used in the catalysis). Samples B2, B3 also include titanium. The share of Ti and O is growing as expected when changing from B2 to B3. Table 1 contains the positions of the main peaks of elements, their half-width (FWHM) and surface area, as well as percentage content of elements.

Sections of spectra for C1s in samples B2 and B3 (Fig. 3, *a, d*) demonstrated the chemical shifts specified for CNTs [44]. These are energy positions for carbon *sp*<sup>2</sup>-hybridization at 284.44 eV and *sp*<sup>3</sup>-hybridization at 285.13 eV. Besides, components are also observed at 286.37 and 288.96 eV, positions of which match the data in paper [45], where they are associated with compounds containing groups C–O–C and O=C–O, accordingly. The peak available at 291.89 eV is caused by losses of energy by photoelectrons for excitation of *π*-plasmons [46]. The section of spectrum for O1s shows that the oxygen is primarily bound by titanium. This is the peak at 530.37 eV. Availability of a small signal of oxygen in groups of C–O–C and O=C–O type manifests itself at 531.78 and



**Figure 1.** SEM images for samples B1 (a), B2 (b) and B3 (c, d) and TEM images for samples B1 (e), B2 (f) and B3 (g).

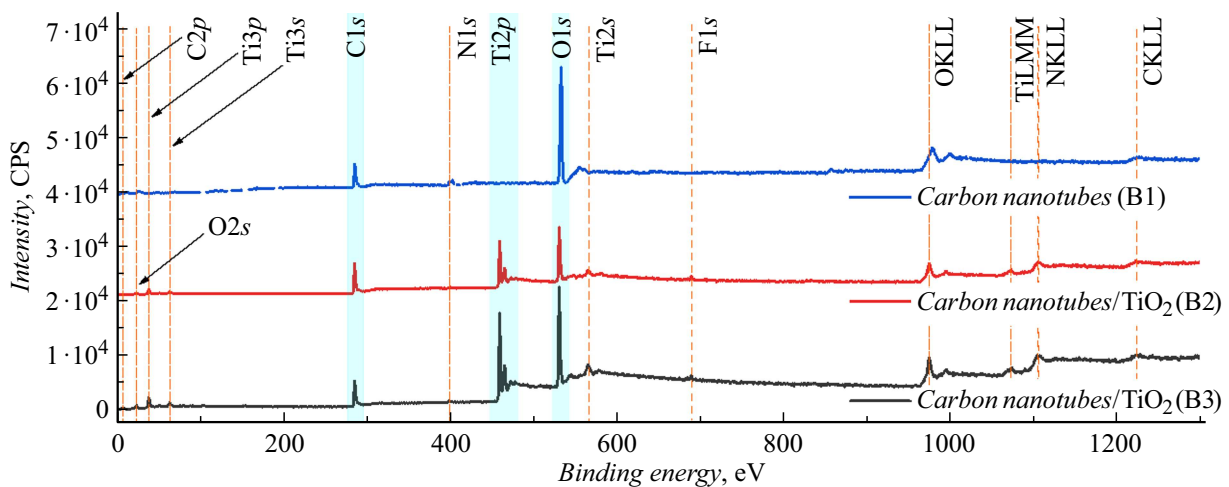


**Figure 2.** XPS for B1, B2 and B3 samples.

532.56 eV accordingly (Fig. 3, b, e). There is a correlation with similar components of the spectrum C1s. Sections of the spectrum for Ti2p of samples B2 and B3 (Fig. 3, c, f) have a typical appearance for TiO<sub>2</sub> [47]. Signals defining the chemical bonds of titanium and oxygen are located at 471.66 and 464.64 eV and relate to Ti2p<sub>3/2</sub> and Ti2p<sub>1/2</sub> accordingly. There is a satellite peak of Ti2p for binding energy 458.94 eV. Processing of spectra for quantitative analysis confirmed that the composition of TiO<sub>2</sub> samples was close to stoichiometric one.

## 2.2. Valence band and work function of sample material

Monitoring of valence band structure and work function of the sample surface demonstrated the following. Spectrum of the valence band of sample B1 (Fig. 4, a) is inherent in CNT [48]. Spectra of valence band for samples B2 and B3 are noticeably different from the first case and are very close to each other. The level of the valence band top (VBT) relative to Fermi edge was 3.11 and 3.13 eV accordingly.

**Table 1.** Chemical composition of sample surface

Peak	Energy of binding, eV	FWHM, eV	Surface area of peak, cps·eV	Content, at. %
B1				
C1s	284.52	1.47	32848	91.04
N1s	400.89	2.78	1437	2.49
O1s	532.14	2.77	6057	6.47
B2				
C1s	284.60	1.63	12978	50.22
Ti2p	458.98	1.44	23692	15.20
O1s	530.44	1.62	22098	32.93
F1s	689.03	1.95	1453	1.65
B3				
C1s	284.69	1.89	12221	33.66
O1s	530.39	1.59	40868	43.34
Ti2p	458.94	1.41	44823	20.47
F1s	689.08	2.88	3134	2.53

Values are specific for type of own conductance of TiO<sub>2</sub>, as well as the dependence type itself [49].

To measure the work function of  $\varphi$ -samples, XPS spectra were used, received in the vicinities of secondary electrons cut-off (Fig. 4, *b*). For B1 the numerical value of work function was 4.98 eV and is in the range specific for CNT 4.32–5.32 eV [50]. Samples B2 and B3 demonstrated lower work function — 4.29 and 3.82 eV accordingly. The difference of values in this pair may be caused by impact of thickness of the oxide film (3 and 6 nm accordingly) on the electronic structure of sample surface. The reduction of the work function as such upon application of TiO<sub>2</sub> on CNT appeared, though to a lower extent (reduction from 4.41 eV for CNT to 4.23 eV upon application of 20 nm TiO<sub>2</sub>), in the early study [51]. Data on work function of ALD layers from TiO<sub>2</sub> on smooth substrates demonstrate values 4.0–4.27 eV [51,52]. Therefore, transition to structures of CNT@TiO<sub>2</sub> type caused expected reduction of electron work function at the expense of the oxide.

### 2.3. Field emission study

At the initial stage of autoemission measurements the samples were exposed to high voltage training (more details about the method in [43]). The nature of dependences (Fig. 5, *a–c*), and also the means for process visualization (see below) show that at this stage the emission centers of the flat cathode were activated and stabilized. Besides, the loss of unstable centers by soft and explosive nature was observed. At each stage the quick CVC was read (the time to record one CVC is equal to 10 ms) with its top for the current at every stage (Fig. 5, *d–f*).

After training, the main complex of measurements was performed. The resulting CVCs of samples had the appearance of Fig. 6, *a* and the following threshold values of field

intensity Eth for the density of emission current 1 mA/cm<sup>2</sup>: 3.11 V/μm for B1, 3.51 V/μm for B2 and 3.16 V/μm for B3. CVC in coordinates of Fowler–Nordheim (FN) equation are given in Fig. 6, *b*. For approximation, Murphy–Good equation was used with Schrednik approximation [53]:

$$I = A_{\text{eff}} \frac{a_{\text{FN}}}{1.1} \varphi^{-1} \alpha_{\text{eff}}^2 U^2 \exp(1.03\eta) \times \exp\left(-0.95 b_{\text{FN}} \varphi^{3/2} \frac{1}{\alpha_{\text{eff}} U}\right), \quad (1)$$

$$\gamma_{\text{eff}} = \alpha_{\text{eff}} d_{\text{sep}}, \quad (2)$$

where  $\eta = b_{\text{FN}} \varphi^{3/2} / F_R = b_{\text{FN}} c_s^2 \varphi^{-1/2}$ ,  $F_R = \varphi^2 c_s^{-2}$  — electric field of barrier removal,  $c_s = 1.439965 \cdot 10^{-9}$  eV<sup>2</sup>·m/V — Schottky constant,  $\alpha_{\text{eff}}$  [1/m] — inverse characteristic length,  $a_{\text{FN}} = 1.541433 \cdot 10^{-6}$  [A·eV/V<sup>2</sup>] and  $b_{\text{FN}} = 6.830890 \cdot 10^9$  [eV<sup>-3/2</sup>·V/m] — first and second Fowler–Nordheim constants,  $\varphi$  — emitter work function [eV],  $\gamma_{\text{eff}}$  — effective field gain factor at emitter's tip,  $A_{\text{eff}}$  — effective surface area of emission,  $U$  — applied voltage. Processing of these dependences makes it possible to assess effective parameters of CNT  $\gamma_{\text{eff}}$  and  $A_{\text{eff}}$  emission. Using CVC of emission in logarithmic coordinates of Fowler–Nordheim, angular coefficient  $K$  and cut-off  $S$  are extracted on the axis of ordinates. Using them, the effective inverse characteristic length  $\alpha_{\text{eff}}$ , emission surface area  $A_{\text{eff}}$  and field gain factor  $\gamma_{\text{eff}}$  on points are recalculated. To process the result of emission tests, values of the work function  $\varphi$  are used, which were obtained previously for each sample by cut-off of secondary electrons with XPS method. I.e. for B1, B2 and B3 the values 4.98, 4.29 and 3.82 eV are accepted accordingly.

The calculated values of the effective gain factor of the field in the row of B1, B2, B3 tend to reduce, which is probably due to change in the geometry of points (for example, increased radius of tube curvature by application of TiO<sub>2</sub>). For a sample with „pure“ CNTs it is close to  $2.53 \cdot 10^3$ , for CNT@TiO<sub>2</sub> (6 nm) it is reduced down to  $1.56 \cdot 10^3$ . It should be noted that reduction of  $\gamma_{\text{eff}}$  is accompanied with growth of  $A_{\text{eff}}$ . When changing from B1 sample, the emission surface area increases noticeably. Average values  $A_{\text{eff}}$  —  $3.12 \cdot 10^3$  nm<sup>2</sup> for B1,  $8.33 \cdot 10^3$  nm<sup>2</sup> for B2 and  $1.31 \cdot 10^4$  nm<sup>2</sup> for B3. Fig. 6, *c* shows the dependence of the emission current on  $F$  — microscopic electric field on the surface of points. For B3 sample with the lowest work function for achievement of the specified threshold of the emission current (1 mA/cm<sup>2</sup>), the lowest electric field was required. Intensity of this field is defined as  $F = \gamma U / d_{\text{sep}}$ , where  $\gamma$  — field gain factor,  $d_{\text{sep}}$  — electrode to electrode distance. It reduces in the row of B1, B2, B3:  $7.89 \cdot 10^9$  V/m,  $5.99 \cdot 10^9$  V/m,  $4.97 \cdot 10^9$  V/m accordingly.

The most important noted parameters of sample emission are summarized in Table 2. It also contains data on the average surface area of the emission center  $\langle A_{\text{site}} \rangle$ . Values are obtained via the number of centers  $N_{\text{site}}$ , which were

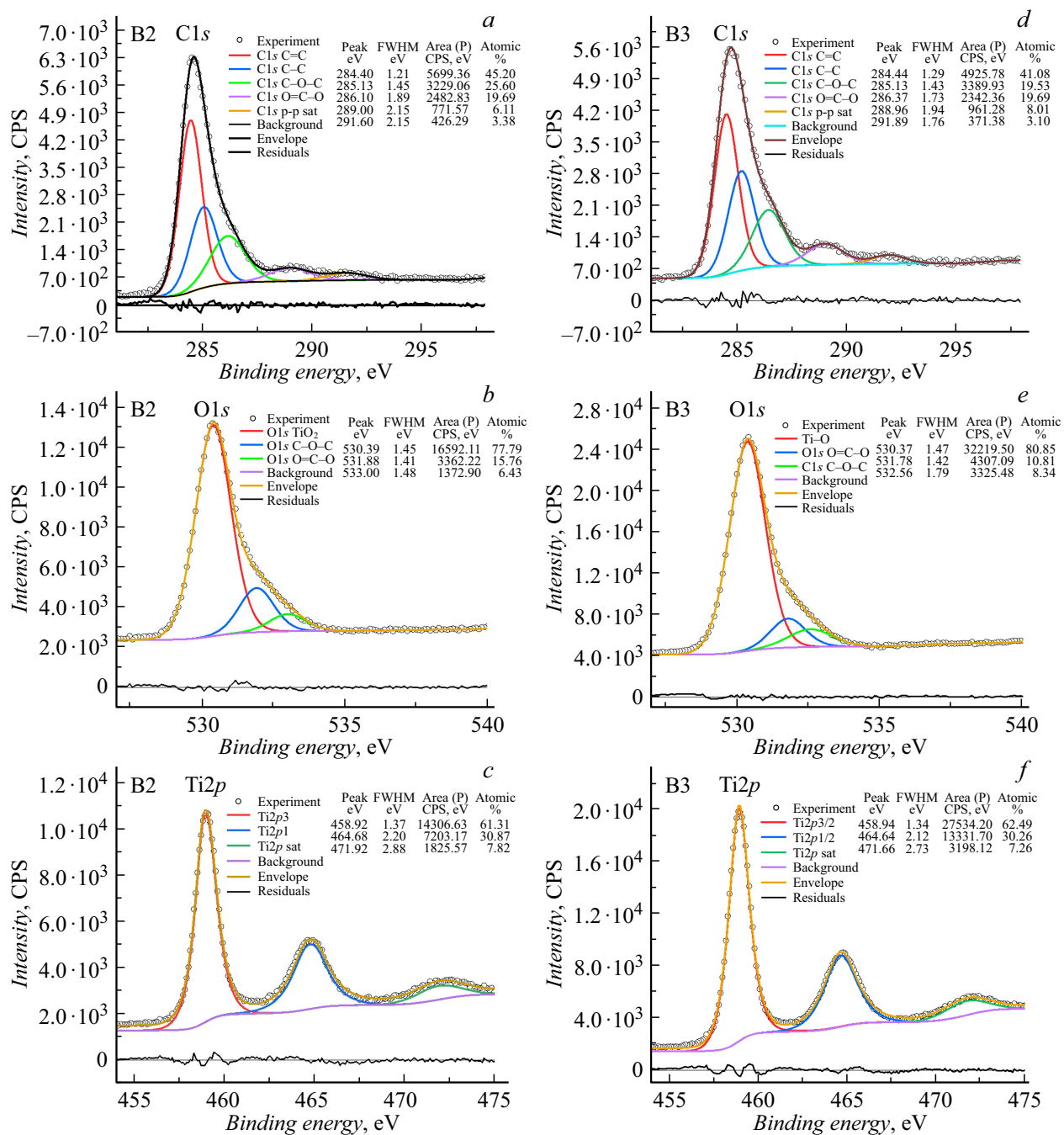


**Figure 3.** XPS sections with peaks C1s, O1s and Ti2p and their deconvolution; for samples B2 (a–c) and B3 (d–f).

**Table 2.** Emission characteristics of samples

No	Sample	$E_{th}$ , V/ $\mu$ m	$U_{max}$ , kV	$I_{max}$ , $\mu$ A	$\alpha_{eff}$ , $m^{-1}$	$\gamma_{eff}$	$\phi$ , eV	$A_{eff}$ , $nm^2$	$\langle A_{site} \rangle$ , $nm^2$
B1	CNT	3.11	1.18	1.53	$6.85 \cdot 10^6$	$2.53 \cdot 10^3$	4.98	$3.12 \cdot 10^3$	4.90
B2	CNT@TiO <sub>2</sub> (3 nm)	3.51	1.34	1.46	$4.61 \cdot 10^6$	$1.70 \cdot 10^3$	4.29	$8.33 \cdot 10^3$	14.02
B3	CNT@TiO <sub>2</sub> (6 nm)	3.16	1.21	1.46	$4.23 \cdot 10^6$	$1.56 \cdot 10^3$	3.82	$1.31 \cdot 10^4$	27.40

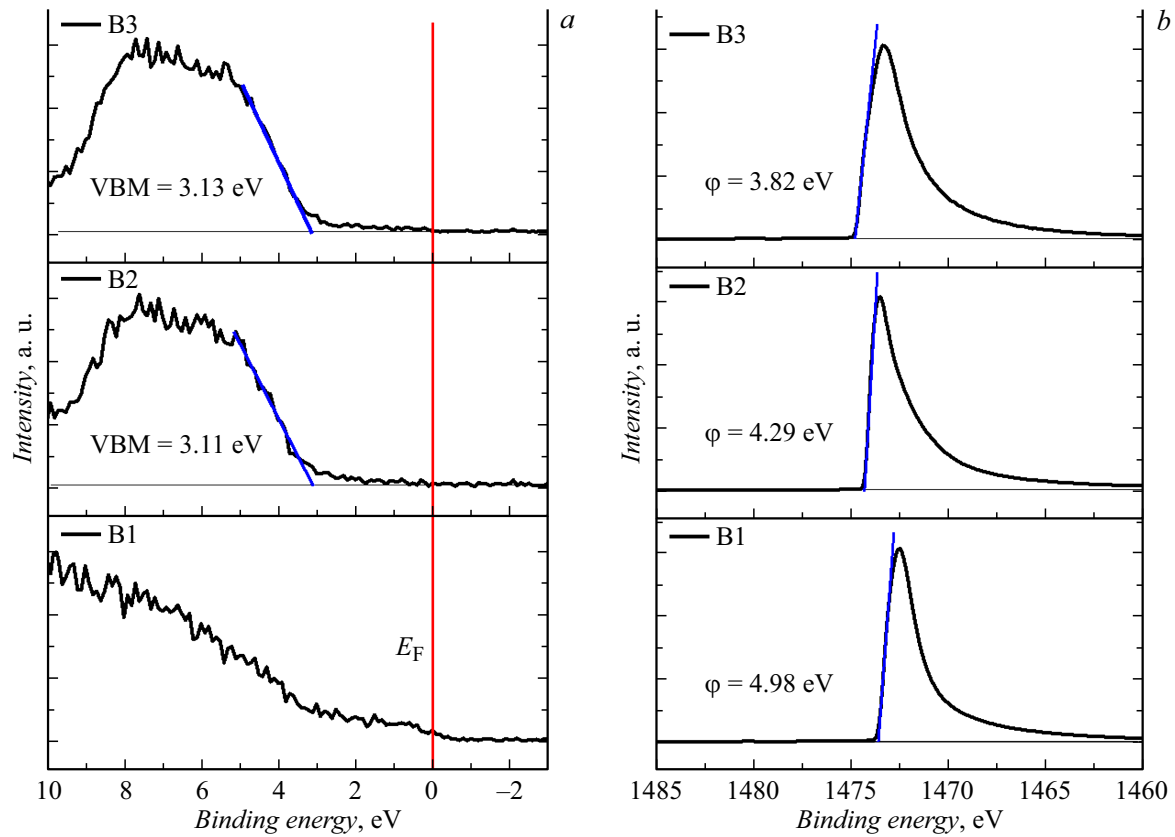


Figure 4. Spectra of valence band (a) and area of secondary electrons cut-off (b) for samples B1, B2 and B3.

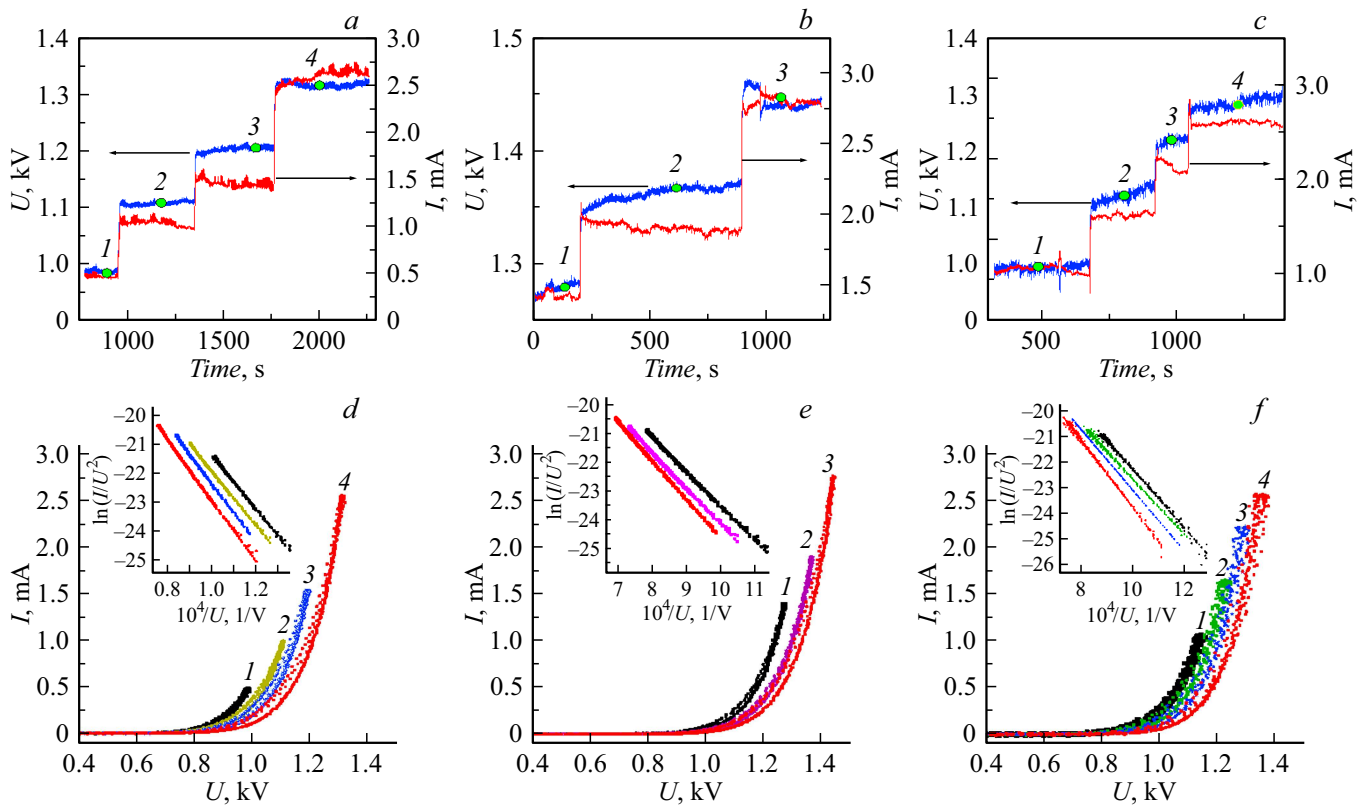
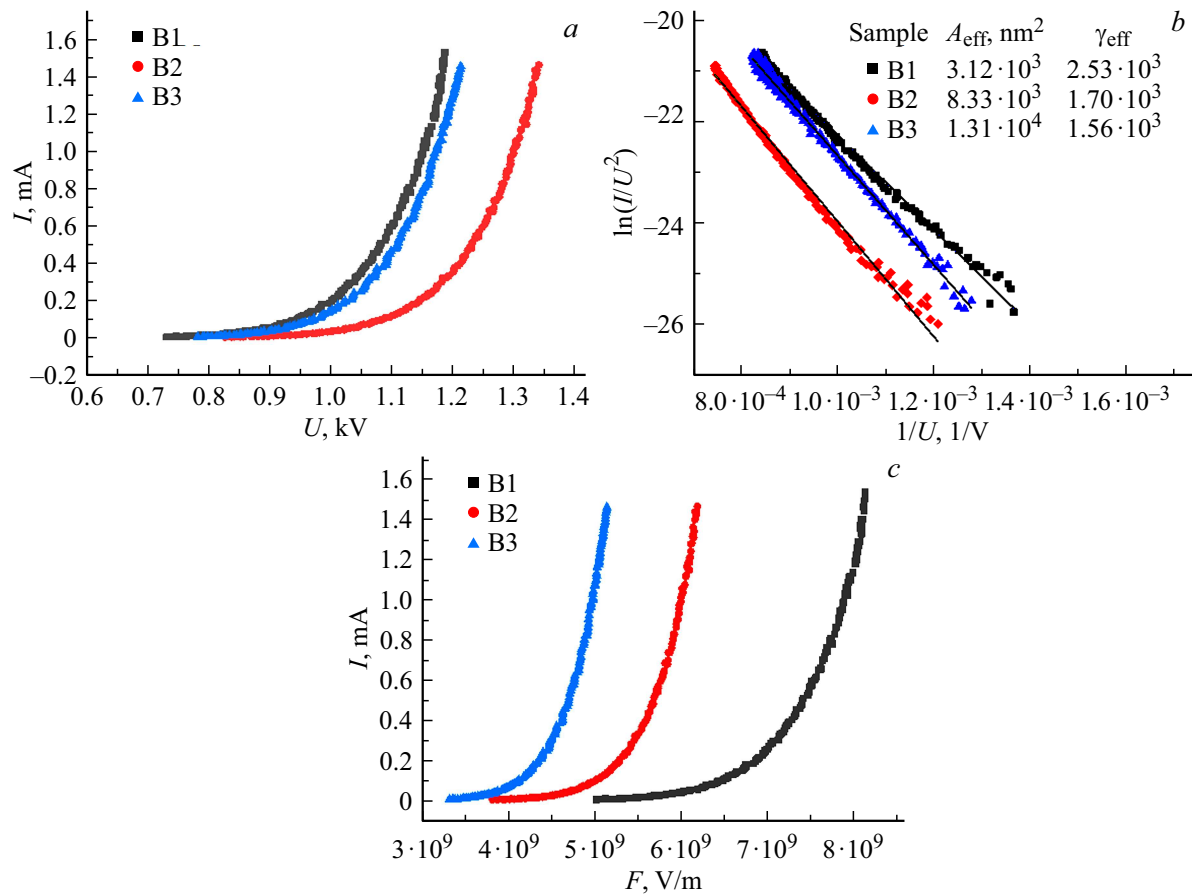
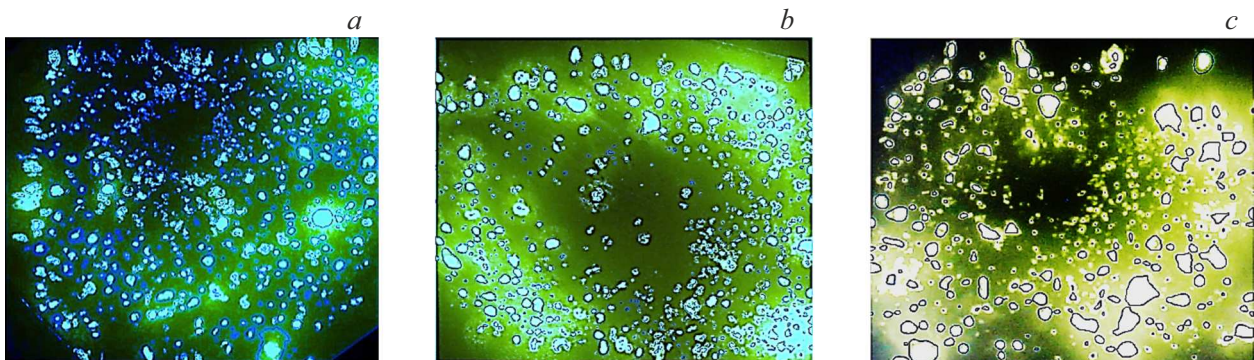


Figure 5. Data of stepwise training of samples B1 (a,d), B2 (b,e), B3 (c,f): a–c — loading characteristics; d–f — CVC (in inserts in coordinates of FN).



**Figure 6.** CVC of emission for samples B1, B2, B3 (a), their corresponding CVCs in FN coordinates (b), current dependence on microscopic field  $F$  on points (c).



**Figure 7.** Photographs of luminescent screen during emission testing of samples B1 ((a), B2 (b) and B3 (c) (actual scan pattern dimensions around  $1 \times 1$  cm).

measured by ITO (Indium Tin Oxide) glass coated with phosphor. It visualized the areas of intense bombardment of the anode with electrons (Fig. 7). At the fixed level of current density ( $1.5 \text{ mA/cm}^{-2}$ ) the luminescence map in general looks the same for all samples. B1 sample had the higher density of emission centers —  $636 \text{ cm}^{-2}$ , for B2 it was 594, for B3 —  $478 \text{ cm}^{-2}$ . A separate glowing spot on the phosphor screen was accepted as such at the selected moment of time. The estimate of the average surface area

of the center ( $\langle A_{\text{site}} \rangle$ ) may be presented as ratio of the sample emission surface area to the number of centers:

$$\langle A_{\text{site}} \rangle = A_{\text{eff}}/N_{\text{site}}. \quad (3)$$

For B1 it was  $4.90 \text{ nm}^2$ , for B2 —  $14.02 \text{ nm}^2$ , for B3 —  $27.40 \text{ nm}^2$ . Therefore, application of TiO<sub>2</sub> caused the increase of both the effective emission surface area of cathode structures and the surface area per single visualized emission center.

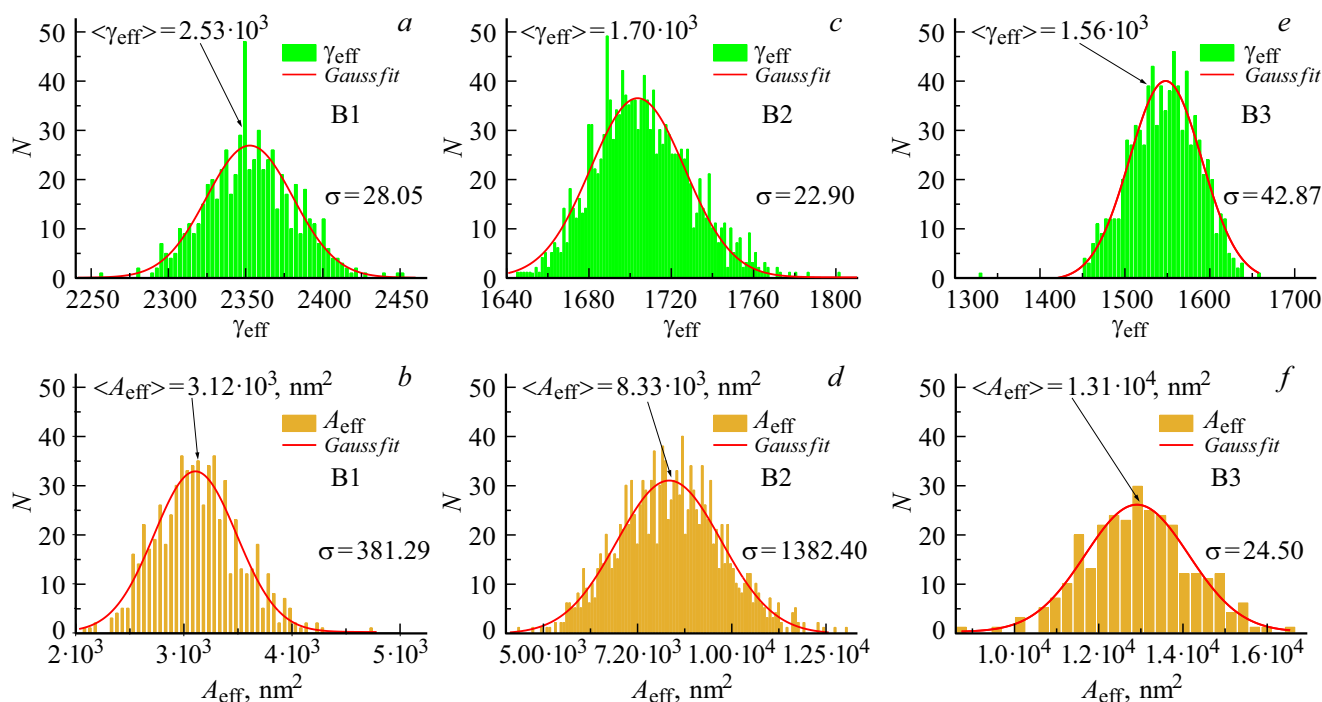


**Figure 8.** Dispersion of gain factor of field  $\gamma_{eff}$  and emission area  $A_{eff}$  for samples B1 (a, b), B2 (c, d) and B3 (e, f).

Further the statistic distributions of fluctuating effective characteristics of field emission  $\gamma_{eff}$  and  $A_{eff}$  for the studied emitters were obtained. The procedure to obtain statistic distributions looked as follows. For nanocomposites, emission CVCs were accumulated, which are recorded with frequency of 20 ms and fluctuate for a certain period of time at the corresponding stages during cathode training. Processing of the data array using equation (1) with account of the measured values of work function made it possible to form histograms of effective parameters. As you can see from Fig. 7, both values for all samples are described with normal distribution. Root-mean-square distribution  $\sigma$  does not have an evident correlation with the conditions of composite modification (see values  $\sigma$  in fields of Fig. 8). Note its obviously low value for  $A_{eff}$  of sample B3. Therefore, the selected criterion of assessment shows that the coating from oxide with thickness of 6 nm substantially stabilizes the surface area of emission in CNT arrays.

## Conclusion

A complex research of the structure, composition, electronic structure of the surface and field emission properties of nanocomposite field radiating cathodes based on CNT arrays coated with an ultrathin layer of  $\text{TiO}_2$  is presented. According to the method of secondary electrons cut-off implemented by XPS, the work function was 4.98 eV for pure CNTs, for  $\text{CNT@TiO}_2$  nanocomposites with the thickness of oxide layer 3 and 6 nm it took on the values of 4.29 and 3.82 eV accordingly. Reduction of the electron work function is probably mainly related to lower work

function of  $\text{TiO}_2$  films vs CNT. The developed method of emission characteristics measurement demonstrated that the reduction of work function for the  $\text{CNT@TiO}_2$  nanocomposites is accompanied by reduction of local electric field on their points: for the structure with the lowest work function ( $\text{CNT@TiO}_2$  (6 nm)), to ensure the density of the emission current  $1 \text{ mA/cm}^2$  the lowest electric field was required, which made  $4.97 \cdot 10^9 \text{ V/m}$ . For comparison, in cathodes with „pure“ CNTs and  $\text{CNT@TiO}_2$  (3 nm) the necessary field was  $7.89 \cdot 10^9$  and  $5.99 \cdot 10^9 \text{ V/m}$  accordingly. Effective field gain factor  $\gamma_{eff}$  for a series of samples tends to reduce when changing from pure CNTs to  $\text{CNT@TiO}_2$  composites, which, probably, to a large extent depends on change in the geometry of points (increased curvature radius). For „pure“ CNTs  $\gamma_{eff}$  is equal to  $2.53 \cdot 10^3$ , and for a sample with the thickest oxide coating it is reduced down to  $1.56 \cdot 10^3$ . It should be noted that drop of  $\gamma_{eff}$  is accompanied by increase of  $A_{eff}$ . When changing from a sample with „pure“ CNTs the emission surface area, average value of  $A_{eff} = 3.12 \cdot 10^3 \text{ nm}^2$ , increases noticeably:  $8.33 \cdot 10^3 \text{ nm}^2$  for  $\text{CNT/TiO}_2$  (3 nm) and  $1.31 \cdot 10^4 \text{ nm}^2$  for  $\text{CNT/TiO}_2$  (6 nm). Besides, application of  $\text{TiO}_2$  resulted in increase of the average area of emission centers. For „pure“ CNTs the average surface area per single center of emission was  $4.90 \text{ nm}^2$ , for  $\text{CNT@TiO}_2$  (3 nm) —  $14.02 \text{ nm}^2$ , for  $\text{CNT@TiO}_2$  (6 nm) —  $27.40 \text{ nm}^2$ . The conducted research demonstrated that application of thin layers of  $\text{TiO}_2$  is promising for increased effectiveness of autoemission cathodes based on CNTs in vacuum nanoelectronics, making it possible to tune the work function of autoemission cathodes.

## Acknowledgments

Equipment provided by the resource center „Physical Methods of Surface Research“ at the Research Park of St. Petersburg University was used in XPS studies.

## Funding

Authors M. Maksimov, L. Filatov and I. Ezhov express gratitude for partial financial support to the Ministry of Science and Higher Education of the Russian Federation (Agreement 075-15-2022-1246 dated October 13, 2022, unique project ID RF-2251.62322X0021).

## Conflict of interest

The authors declare that they have no conflict of interest.

## References

- [1] N.L. Rupesinghe, M. Chhowalla, K.B.K. Teo, G.A.J. Amaratunga. *J. Vacuum Sci. Technol. B*, **21** (1), 338 (2003). DOI: 10.1116/1.1527635
- [2] R. Rosen, W. Simendinger, C. Debbault, H. Shimoda, L. Fleming, B. Stoner, O. Zhou. *Appl. Phys. Lett.*, **76** (13), 1668 (2000). DOI: 10.1063/1.126130
- [3] G. Z. Yue, Q. Qiu, B. Gao, Y. Cheng, J. Zhang, H. Shimoda, J.P. Lu, O. Zhou. *Appl. Phys. Lett.*, **81** (2), 355 (2002). DOI: 10.1063/1.1492305
- [4] J.W. Jeong, J.W. Kim, J.T. Kang, S. Choi, S. Ahn, Y.H. Song. *Nanotechnology*, **24** (8), 085201 (2013). DOI: 10.1088/0957-4484/24/8/085201
- [5] S.H. Heo, A. Ihsan, S.O. Cho. *Appl. Phys. Lett.*, **90** (18), 183109 (2007). DOI: 10.1063/1.2735549
- [6] S.H. Heo, H.J. Kim, J.M. Ha, S.O. Cho. *Nanoscale Res. Lett.*, **7**, 1 (2012). DOI: 10.1186/1556-276X-7-258
- [7] N.S. Lee, D.S. Chung, J.H. Kang, H.Y. Kim, S.H. Park, Y.W. Jin, J.M. Kim. *Jpn. J. Appl. Phys.*, **39** (12S), 7154 (2000). DOI: 10.1143/JJAP.39.7154
- [8] K. Jiang. *Industrial Applications Carbon Nanotubes*, 101 (2017). DOI: 10.1016/B978-0-323-41481-4.00004-6
- [9] W. Knapp, D. Schleussner, A.S. Baturin, I.N. Yeskin, E.P. Sheshin. *Vacuum*, **69** (1-3), 339 (2002). DOI: 10.1016/S0042-207X(02)00355-X
- [10] E.P. Sheshin, A.Y. Kolodyazhnyj, N.N. Chadaev, A.O. Getman, M.I. Danilkin, D.I. Ozol. *J. Vacuum Sci. Technol. B*, **37** (3), 031213 (2019). DOI: 10.1116/1.5070108
- [11] S.T. Yoo, J.Y. Lee, A. Rodiansyah, T.Y. Yune, K.C. Park. *Current Appl. Phys.*, **28**, 93 (2021). DOI: 10.1016/j.cap.2021.05.007
- [12] Z. Wen, Y. Wu, Z. Zhang, S. Xu, S. Huang, Y. Li. *Sensors and Actuators A: Physical*, **103** (3), 301 (2003). DOI: 10.1016/S0924-4247(02)00392-8
- [13] S. Kang, W. Qian, R. Liu, H. Yu, W. Zhu, X. Liao, F. Wang, W. Huang, Ch. Dong. *Vacuum*, **207**, 111663 (2023). DOI: 10.1016/j.vacuum.2022.111663
- [14] Y. Kanazawa, T. Oyama, K. Murakami, M. Takai. *J. Vacuum Sci. Technol. B*, **22** (3), 1342 (2004). DOI: 10.1116/1.1667518
- [15] A. Sawada, M. Iriguchi, W.J. Zhao, C. Ochiai, M. Takai. *J. Vacuum Sci. Technol. B*, **21** (1), 362 (2003). DOI: 10.1116/1.1527597
- [16] G. Chai, L. Chow, D. Zhou, S.R. Byahut. *Carbon*, **43** (10), 2083 (2005). DOI: 10.1016/j.carbon.2005.03.009
- [17] D.H. Kim, C.D. Kim, H.R. Lee. *Carbon*, **42** (8-9), 1807 (2004). DOI: 10.1016/j.carbon.2004.03.015
- [18] J.D. Hwang, K.F. Chen, L.H. Chan, Y.Y. Chang. *Appl. Phys. Lett.*, **89** (3), 033103 (2006). DOI: 10.1063/1.2222337
- [19] J.Y. Pan, C.C. Zhu, Y.L. Gao. *Appl. Surf. Sci.*, **254** (13), 3787 (2008). DOI: 10.1016/j.apsusc.2007.12.002
- [20] X. Yan, B.K. Tay, P. Miele. *Carbon*, **46** (5), 753 (2008). DOI: 10.1016/j.carbon.2008.01.027
- [21] S. Chakrabarti, L. Pan, H. Tanaka, S. Hokushin, Y. Nakayama. *Jpn. J. Appl. Phys.*, **46** (7R), 4364 (2007). DOI: 10.1143/JJAP.46.4364
- [22] C. Yang, Y. Li-Gang, W. Ming-Sheng, Z. Qi-Feng, W. Jin-Lei. *Chin. Phys. Lett.*, **22** (4), 911 (2005). DOI: 10.1088/0256-307X/22/4/037
- [23] H.B. Lian, K.Y. Lee, K.Y. Chen, Y.S. Huang. *Diamond and Related Materials*, **18** (2-3), 541-543 (2009). DOI: 10.1016/j.diamond.2008.10.054
- [24] C.A. Chen, K.Y. Lee, Y.M. Chen, J.G. Chi, S.S. Lin, Y.S. Huang. *Vacuum*, **84** (12), 1427 (2010). DOI: 10.1016/j.vacuum.2009.12.016
- [25] M. Sreekanth, S. Ghosh, P. Srivastava. *arXiv* (2018). *arXiv preprint*. DOI: 10.48550/arXiv.1811.10951
- [26] C.J. Yang, J.I. Park, Y.R. Cho. *Adv. Eng. Mater.*, **9** (1-2), 88 (2007). DOI: 10.1002/adem.200600003
- [27] Y.M. Chen, C.A. Chen, Y.S. Huang, K.Y. Lee, K.K. Tiong. *Nanotechnology*, **21** (3), 035702 (2009). DOI: 10.1088/0957-4484/21/3/035702
- [28] Y.M. Chen, C.A. Chen, Y.S. Huang, K.Y. Lee, K.K. Tiong. *J. Alloys and Compounds*, **487** (1-2), 659 (2009). DOI: 10.1016/j.jallcom.2009.07.181
- [29] Y. Il Song, C.M. Yang, L. Ku Kwac, H. Gun Kim, Y. Ahm Kim. *Appl. Phys. Lett.*, **99** (15), 153115 (2011). DOI: 10.1063/1.3650471
- [30] J. Xu, P. Xu, W. Ou-Yang, X. Chen, P. Guo, J. Li, X. Piao, M. Wang, Z. Sun. *Appl. Phys. Lett.*, **106** (7), 073501 (2015). DOI: 10.1063/1.4909552
- [31] M.M. Raza, M. Sadiq, S. Khan, M. Zulfequar, M. Husain, S. Husain, J. Ali. *Diamond and Related Mater.*, **110**, 108139 (2020). DOI: 10.1016/j.diamond.2020.108139
- [32] P.H. Chen, Y.S. Huang, W.J. Su, K.Y. Lee, K.K. Tiong. *Mater. Chem. Phys.*, **143** (3), 1378 (2014). DOI: 10.1016/j.matchemphys.2013.11.049
- [33] R. Smoluchowski. *Phys. Rev.*, **60** (9), 661 (1941). DOI: 10.1103/PhysRev.60.661
- [34] W. Li, D.Y. Li. *J. Chem. Phys.*, **122** (6), 064708 (2005). DOI: 10.1063/1.1849135
- [35] R.W. Strayer, W. Mackie, L.W. Swanson. *Surface Sci.*, **34** (2), 225 (1973). DOI: 10.1016/0039-6028(73)90117-9
- [36] A. Jablonski, K. Wandelt. *Surface Interface Analysis*, **17** (9), 611 (1991). DOI: 10.1002/sia.740170902
- [37] M.T. Greiner, L. Chai, M.G. Helander, W.M. Tang, Z.H. Lu. *Adv. Functional Mater.*, **22** (21), 4557 (2012). DOI: 10.1002/adfm.201200615
- [38] S. Lany, J. Osorio-Guillén, A. Zunger. *Phys. Rev. B*, **75** (24), 241203 (2007). DOI: 10.1103/PhysRevB.75.241203
- [39] M.T. Greiner, M.G. Helander, Z.B. Wang, W.M. Tang, Z.H. Lu. *J. Phys. Chem. C*, **114** (46), 19777 (2010). DOI: 10.1021/jp108281m

- [40] L. Filatov, P. Vishniakov, I. Ezhov, I. Gorbov, D. Nazarov, D. Olkhovskii, R. Kumar, S. Peng, G. He, V. Chernyavsky, M. Gushchina, M. Maximov. *Mater. Lett.*, **353**, 135250 (2023). DOI: 10.1016/j.matlet.2023.135250
- [41] M.A. Chumak, A.A. Rokacheva, L.A. Filatov, A.G. Kolosko, S.V. Filippov, E.O. Popov. *J. Phys.: Conf. Series. — IOP Publishing*, **2103** (1), 012110 (2021). DOI: 10.1088/1742-6596/2103/1/012110
- [42] R. Schlaf, H. Murata, Z.H. Kafafi. *J. Electron Spectr. Related Phenomena*, **120** (1–3), 149 (2001). DOI: 10.1016/S0368-2048(01)00310-3
- [43] E.O. Popov, A.G. Kolosko, S.V. Filippov, E.I. Terukov, R.M. Ryazanov, E.P. Kitsyuk. *J. Vacuum Sci. Technol. B*, **38** (4), 043203 (2020). DOI: 10.1116/6.0000072
- [44] M. Scardamaglia, M. Amati, B. Llorente, P. Mudimela, J.F. Colomer, J. Ghijsen, C. Ewels, R. Snyders, L. Gregoratti, C. Bittencourt. *Carbon*, **77**, 319 (2014). DOI: 10.1016/j.carbon.2014.05.035
- [45] T.I.T. Okpalugo, P. Papakonstantinou, H. Murphy, J. McLaughlin, N.M.D. Brown. *Carbon*, **43** (1), 153 (2005). DOI: 10.1016/j.carbon.2004.08.033
- [46] Y.M. Shulga, T. Ta-Chang, H. Chi-Chen, L. Shen-Chuan, V.E. Muradyan, N.F. Polyakova, L. Yong-Chien. *Alternative Energy and Ecology*, **10**, 40 (2006).
- [47] A. Kemelbay, A. Tikhonov, S. Aloni, T.R. Kuykendall. *Nanomaterials*, **9** (8), 1085 (2019). DOI: 10.3390/nano9081085
- [48] A. Dobrzańska-Danikiewicz, D. Łukowiec, J. Kubacki. *J. Nanomaterials*, **2016**. DOI: 10.1155/2016/4942398
- [49] X. Chen, L. Liu, Z. Liu, M.A. Marcus, W.C. Wang, N.A. Olyer, M.E. Grass, B. Mao, P.-A. Glans, P.Y. Yu, J. Guo, S.S. Mao. *Scientific Reports*, **3** (1), 1510 (2013). DOI: 10.1038/srep01510
- [50] R. Kumari, P.K. Tyagi, N.K. Puri. *Appl. Phys. A*, **124**, 1 (2018). DOI: 10.1007/s00339-018-1850-8
- [51] A. Moya, N. Kemnade, M.R. Osorio, A. Cherevan, D. Granados, D. Eder, J.J. Vilatela. *J. Mater. Chem. A*, **5** (47), 24695 (2017). DOI: 10.1039/C7TA08074C
- [52] J. Jhaveri. *Interface Recombination in TiO<sub>2</sub>/Silicon Heterojunctions for Silicon Photovoltaic Applications* (Doctoral dissertation, Princeton University, 2018)
- [53] V.N. Shrednik. *Field Emission Theory*. (Chap. 6. In *Unheated Cathodes*; Elinson, M.I., Ed.; Sovetskoe Radio: M., Russia, 1974), p. 165–207. (In Russian)

*Translated by M.Verenikina*